Heliyon 8 (2022) e11088

Contents lists available at ScienceDirect

Heliyon

journal homepage: www.cell.com/heliyon

Research article

Synthesis and characterization of silver-indium and antimony selenide: role in photocatalytic degradation of dyes

N. Yasmin [a,1], A. Liaqat [a,b,1], G. Ali [b], A. Kalsoom [c], M. Safdar [d,**], M. Mirza [a,*]

[a] Department of Physics the Women University Multan 66000, Pakistan
[b] U.S.-Pakistan Center for Advanced Studies in Energy (USPCAS-E) National University of Science and Technology (NUST), Islamabad 44000, Pakistan
[c] Department of Physics Govt. Sadiq College Women University, Bahawalpur 63100, Pakistan
[d] Department of Basic Sciences & Humanities Khawaja Fareed University of Engineering & Information Technology, Rahim Yar Khan 64200, Pakistan

ARTICLE INFO

Keywords:
Hydrothermal
UV-Vis-spectroscopy
Photocatalytic activity

ABSTRACT

These days, water contamination poses a severe threat to the ecosystem and demands immediate care. This study examined the need to reduce water pollution using clean, renewable energy (solar light irradiations) for the degradation of Congo red by Silver-indium and antimony selenide with chemical composition $AgInSbSe_3$. The sample was fabricated through a hydrothermal technique. The synthesized sample was characterized through X-ray diffraction (XRD), Fourier-transform infrared spectroscopy (FTIR), Scanning electron microscopy (SEM) and Ultraviolet-Visible spectroscopy. The X-ray diffraction confirms crystalline structure of the synthesized sample. The SEM analysis reveals irregular grains and exhibits a very small inter-particle distance. SEM provides the morphology of the synthesized sample, the grain size of the synthesized sample was 0.58 μm. FTIR results revealed specific absorption bands in the range of 400–4000 cm^{-1}; optical properties are studied through UV-Vis-spectroscopy. The synthesized sample has 1.97 eV bandgap which is suitable for degradation of organic pollutants. The photocatalytic activity of the material is checked by degrading the Congo red dye under direct sunlight irradiation and for the 75 min illumination 77.8% degradation efficiency is attained.

1. Introduction

The presence of numerous organic dyes in industrial effluents contributes to water contamination. The textile industry uses 10–12% of all organic dyes annually [1, 2]. According to reports, during dye manufacturing and processing, 20% of these dyes are released into the water. Due to the presence of dangerous dyes, such industrial effluents have detrimental impacts on both humans and aquatic species. These dyes are difficult to remove from wastewater because they are non-biodegradable, carcinogenic, oxidizing agents and stable to light [3, 4]. Therefore, it is crucial to clean the waste water before releasing it into the environment. These chemicals are degraded using various conventional waste water treatment techniques like bioadsorption [5], catalytic reduction [6], coagulation [7], membrane filtration [8], adsorption [9, 10], ion exchange removal [11, 12], photocatalytic degradation [13, 14], ozonation [15] and biological/aerobic treatment [16]. Over the past few years, photodegradation of pollutants has become incredibly popular [17, 18, 19, 20, 21]. Researchers have been significantly more intrigued by photocatalytic technology than the others due to its sustainability, efficient use of solar energy and eco friendly nature. The photocatalytic reaction involves photocatalysis, where a semiconductor photocatalyst absorbs light (artificial light or sun light) to break down a variety of environmental pollutants, such as organic pollutants in the water and the air. When compared to conventional wastewater treatment techniques, photodegradation has advantages. For instance, at room temperature, active photocatalysts can completely degrade organic contaminants in a few hours. Additionally, organic contaminants can entirely mineralize into relatively safe products (water and CO_2) without the development of secondary harmful compounds [22, 23]. Surface functionalization of nanoparticles is used for effective degradation of hazardous contaminants through photodegradation [24, 25].

For photocatalysis, a variety of photoactive substances have been studied, including metal nanoparticles, metal graphene oxides, metal encapsulated biopolymers, metal sulfides, and other functional materials.

* Corresponding author.
** Corresponding author.
E-mail addresses: safdarsami@yahoo.com (M. Safdar), misbahmirza88@yahoo.com (M. Mirza).
[1] authors equally contribute for this manuscript.

https://doi.org/10.1016/j.heliyon.2022.e11088
Received 3 December 2021; Received in revised form 9 March 2022; Accepted 10 October 2022

Numerous studies have been done on the use of metal oxides in heterogeneous catalysis for the degradation of organic dyes. Doping to increase the catalyst's photocatalytic activity was also taken into consideration for considerable degradation. Increasing interests in chalcogenides-based semiconducting materials are extensively used nowadays in photodetectors, photovoltaic devices and photocatalytic degradation. However, a path for selenides has emerged through time. In the form of binary selenides with transition metals, selenium, a semiconductor, is frequently utilized in contemporary instruments including electrodes, photoconductors, and electrical or optical devices [25, 26, 27, 28, 29, 30, 31, 32]. A lot of multinary metal selenides have been discussed to study the photocatalytic effect like, $AgInSe_2$, $AgInSe_2/TiO_2$ [33], $Sb_2Se_3/\beta In_2Se_3$ [34], CdSe@CA, Ag–CdSe@CA, CdSe/GO@CA, Ag–CdSe/GO@CA [35], CdSe/CdS, CdSe/CdS/ZnS [36], CdSe [37], Ag5Sn4Se12]•3H_2O [38].

Congo red (CR) which is benzidine-based diazo dye with anionic nature has usage in plastic, textile, printing and paper industries, raises concerns about water contamination due to its mutagenic and carcinogenic properties. Due to its stability and intricate structure, it is extremely resistant to deterioration. So it's necessary to synthesis such materials which are easily available, abundant in nature, eco-friendly and energy saving to degrade such harmful organic pollutants like CR dye. Herein we fabricated the selenide-based composite through hydrothermal technique. This technique is easy to deal and fast to synthesize the required nanomaterials. The obtained material was characterized through XRD, FTIR, SEM and UV-spectroscopy. This composite is active photocatalyst for organic pollutants because it is non-toxic and absorbs both visible and UV light well. Our fabricated ternary selenide composite has a band gap of 1.97eV. The synthesized photocatalysts had shown good efficiency for degradation of CR dye under direct sunlight. This research expands the range of uses for metal based chalcogenides, which were previously limited to semiconducting applications and this research will help to develop additional photocatalysts from the chalcogenide family.

2. Experimental details

2.1. Chemicals

To investigate this study following chemicals with their maximum purity has been used. $SbCl_3$ (Merck ≥99%), hydrazine solution (in H_2O solution ~80%), ethanol (sigma Aldrich 99.6%), Na_2SeO_3 (Merck >99%), EDA (UNI CHEM 95.0%), silver nitrate (Sigma Aldrich ≥99%), NaOH (≥97.0%), KOH (99% Pub Chem), $In(NO_3)_3$ (99.9% Sigma Aldrich) and deionized water. All the obtained chemicals have maximum purity and are used without any purification.

2.2. Sample synthesis technique

The synthesized sample $AgInSbSe_3$ was synthesized by using hydrothermal technique. In beaker A 3ml HCl+5ml H_2O was added and placed on magnetic rotor for continuous stirring. Then 1g NaOH+10ml H_2O was added. After the above mixture was dissolved $In(NO_3)_3$ (0.22g) and $AgNO_3$ (0.179g) was added with continuous stirring for 2 h at 60°C. After stirring for half an hour, the pH was checked that was 1. To maintain the pH at 7, 5ml H_2O and 3ml hydrazine was added. In beaker B 10ml EDA + Na_2SeO_3 (0.52g) was added with continuous stirring on magnetic stirrer for 30 min. After this, all solutions were mixed in single beaker and were put on magnetic stirrer for 20 min. Then the pH was checked, that was exactly 11. The mixture was poured in autoclave and the autoclave was placed in oven for 24 h at 200°C. Then the sample was filtered and washed with de-ionized water for 3–4 times and then with ethanol. To attain the sample in powder form the sample was placed in oven for 2 h at 180°C. The sample was then grounded with pastel and mortar for 20 min Figure 1 illustrated schematic diagram of the synthesis of $AgInSbSe_3$ through hydrothermal technique.

2.3. Characterization techniques

X-ray diffraction of powder sample was performed through on Bruker D Z Phaser (PW1830) with Cu-Ka radiation of λ (k =) 1.54 Å, at a 2°/min speed of scan. Morphology of synthesized sample is studied via EDX and SEM through Hitachi SU 3500. FTIR spectrum at room temperature is attained from Nicolet 6700 by KBr disk technique in the range of 500–3500 cm^{-1}. The UV spectroscopy is carried out through AE-S90-2D UV spectrometer.

2.4. Photocatalytic activity

To investigate the photocatalytic proficiency of synthesized $AgInSbSe_3$, Congo red (CR) dye was used as a target organic pollutant. Firstly prepare 10 ppm solution of CR in 100 ml of deionized water and add 0.02 g of catalyst under continuous stirring on magnetic plate and after it put this under dark for 30 min to achieve adsorption-desorption equilibrium among molecules of dye and photocatalyst. After 30 min of dark absorbance was checked through UV-visible spectrophotometer.

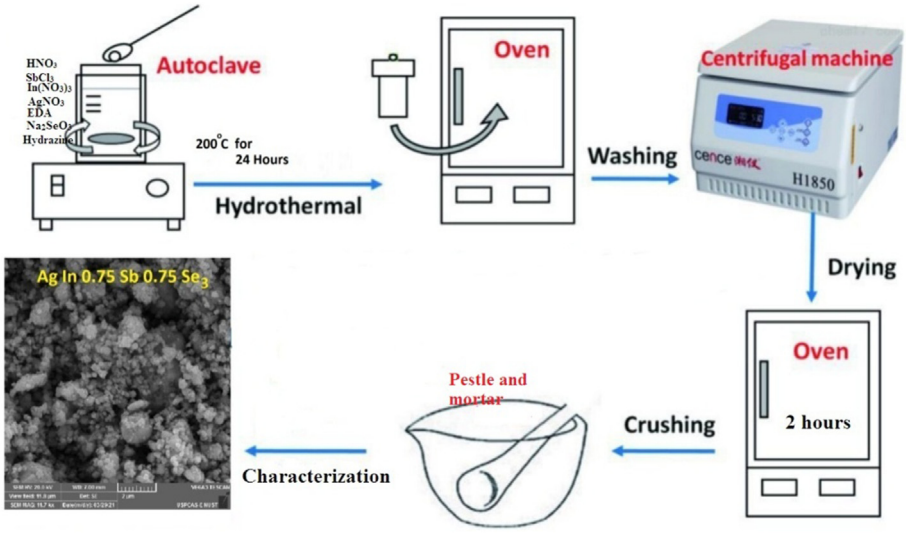

Figure 1. Schematic diagram of the synthesis of $AgInSbSe_3$ through hydrothermal technique.

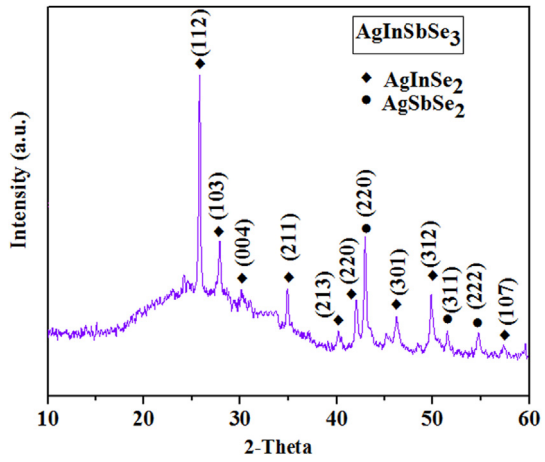

Figure 2. XRD pattern of $AgInSbSe_3$ ternary chalcogenides.

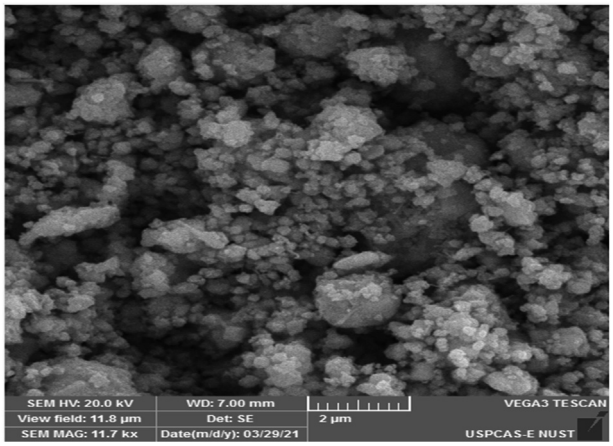

Figure 3. SEM image of synthesized $AgInSbSe_3$ composite.

Then put this solution under direct sunlight to check its absorbance for 75 min under continuous stirring. Take out 3 ml of sample after every 15 min and centrifuged the sample for 7–8 min to remove the catalyst from it and check its absorbance and determined the photocatalytic efficiency of the catalyst.

3. Results and discussions

3.1. Analysis of XRD spectrum

The graph is plotted between the angle range set between 10-70° and the intensity as represented in Figure 2. The XRD of the synthesized silver indium and antimony selenide reveals that the sample is crystalline. In our synthesized composite basically ternary phase is observed which are $AgInSe_2$ and $AgSbSe_2$. The peaks are matched with two JCPDs card No 01-075-0118 and 00-012-0379. The peaks show the hkl values that basically the evidence of the size and structure of the crystal; hence the values are (112) (103), (004) (211), (213) (220), (220) (301), (312) (311), (222) and (107) [39, 40, 41, 42].

The size of crystallites was estimated from the following below relation

$$D = k\,\lambda/\beta\cos\theta \tag{1}$$

Here in the above equation D denotes the crystallite magnitude, λ is wavelength of used X-ray (1.54 Å), β is the full width at half maxima in radian, and θ is the angle, K is constant [42]. The average calculated crystallite sizes for $AgInSe_2$ and $AgSbSe_2$ are mentioned in Table 1. The lattice parameters, volume, X-ray density, dislocation density and micro strain are calculated with the help of the following Eqs. (2), (3), (4), (5), (6), and (7) respectively:

For Tetragonal structure

$$\frac{1}{d^2} = \frac{h^2+k^2}{a^2} + \frac{l^2}{c^2} \tag{2}$$

$$V = a^2c \tag{3}$$

For Cubic

$$\alpha = d_{hkl}\left(h^2+k^2+l^2\right)^{1/2} \tag{4}$$

$$V = \alpha^3 \tag{5}$$

$$\delta = \frac{1}{d^2} \tag{6}$$

$$\varepsilon = \frac{\beta}{4\tan\theta} \tag{7}$$

Calculated values of lattice parameters, volume, X-ray density, dislocation density and micro strain for $AgInSe_2$ and $AgSbSe_2$ are mentioned in Table 1.

3.2. SEM and EDX analysis

The SEM micrograph of the prepared sample $AgInSbSe_3$ shows that grains cover the entire homogeneous surface in micrometer scale as shown in Figure 3. The SEM image shows irregular grains, which are

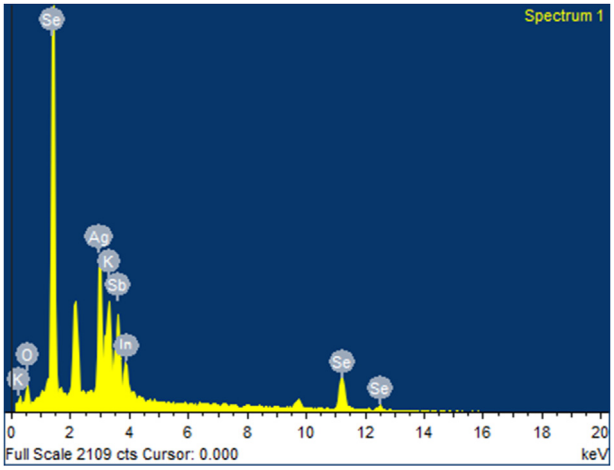

Figure 4. EDX of synthesized sample contain silver, indium, antimony and selenide peaks.

Table 1. Crystallite size, lattice parameters, volume, dislocation density and micro strain for $AgInSe_2$ and $AgSbSe_2$.

Sr. No.	Crystallite size (nm)	Lattice parameters (Å)	Volume (Å^3)	Dislocation density nm^{-2}	Micro strain	X-ray density g/cm^3
$AgInSe_2$	19.04	a = b = 6.06, c = 12	440.6	2.7×10^{-3}	0.55	6.77
$AgSbSe_2$	8.07	a = b = c = 5.77	192.10	1.54×10^{-2}	2.01	10.06

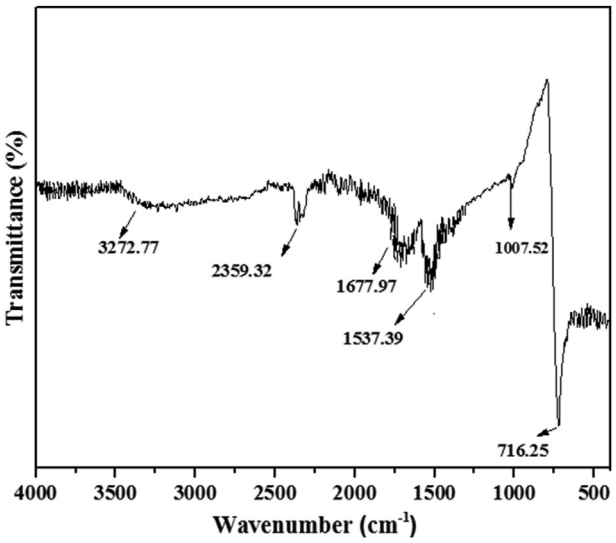

Figure 5. FTIR spectra image of $AgInSbSe_3$.

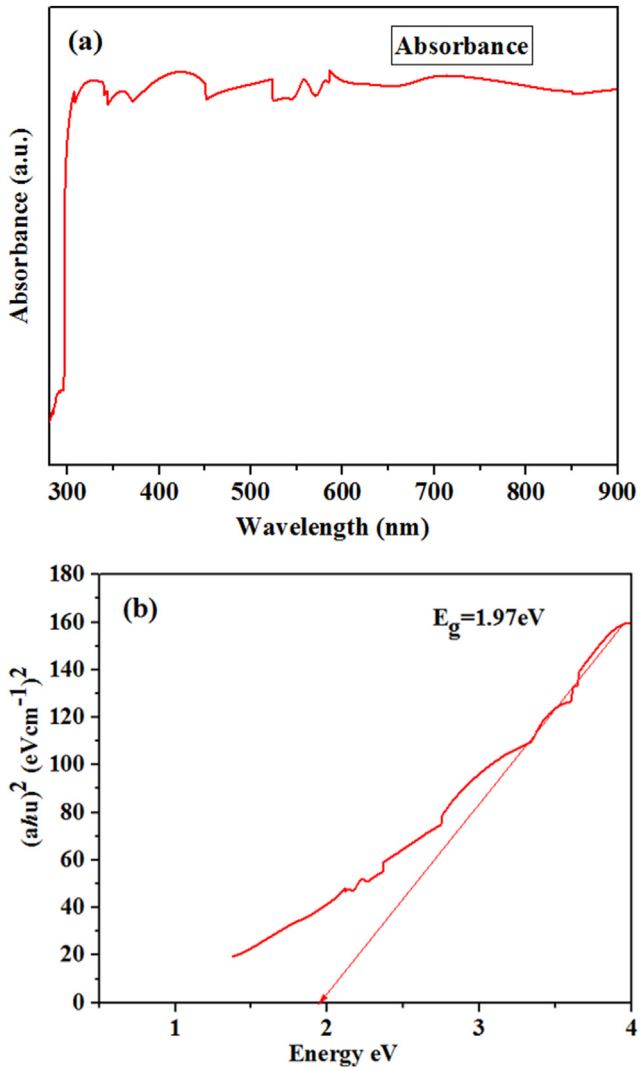

Figure 6. a. Absorption spectra of synthesized sample. b. Illustration of band gap using Tauc equation.

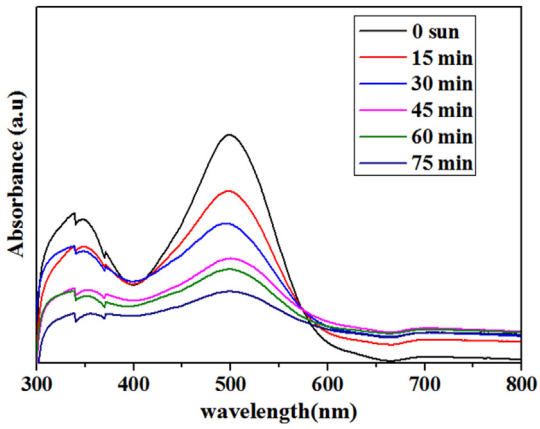

Figure 7. Photocatalytic efficiency of $AgInSbSe_3$ under direct sunlight.

diffused and exhibit a very small inter-particle distance. The grain size measured that is 0.58 μm. EDX of the prepared sample is shown in Figure 4 and it illustrated the elemental composition of the material.

3.3. FTIR

FTIR of the synthesized sample is shown in Figure 5. The graph is plotted between the transmittance and wave number ranging 400-4000 cm^{-1}. In Figure 5 the bands are appeared at 3272.77 cm^{-1}, 2359.32 cm^{-1}, 1677.97 cm^{-1}, 1537.39 cm^{-1}, 1007.52 cm^{-1}, 716.25 cm^{-1} and 459.09 cm^{-1}. The bands at around 3272.77 cm^{-1}, 2359.32 cm^{-1} and 1677.97 cm^{-1} are due to the silver ion binding with hydroxyl or N–H (amine), C–H (hydrocarbons stretching) and C=O vibrational stretching respectively [43]. The band appeared at around 1537.39 cm^{-1} is attributed to the N–H bond stretching [44]. While the absorption at 1007.52 cm^{-1} is assigned to the vibrational mode associated with mixed vibration due to C–N bonding [45], while the band at 716.25 indicates to $–CSe_2$out of phase stretching [44].

3.4. Optical properties

To study the optical properties of the synthesized sample absorbance of the composite is checked by using UV-Vis-spectrophotometer and Figure 6(a) illustrated the absorbance spectrum of the composite. While, to estimate the band gap Eq. (8) is used because the energy band gap is an important factor in catalytic activity of a catalyst and its value is calculated from the Tauc plot which is shown in Figure 6(b) and it is drawn

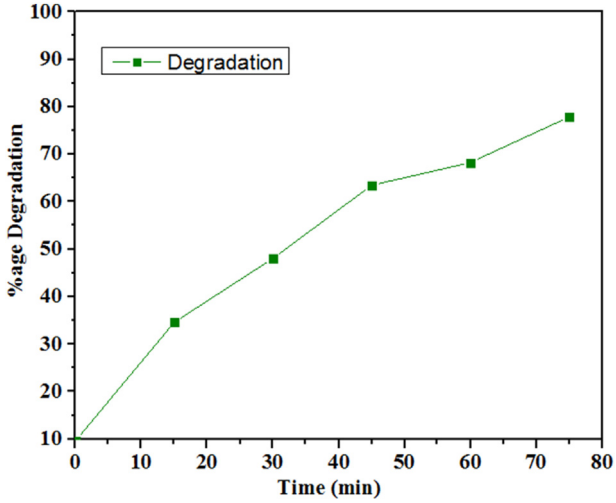

Figure 8. %age degradation efficiency of the prepared sample.

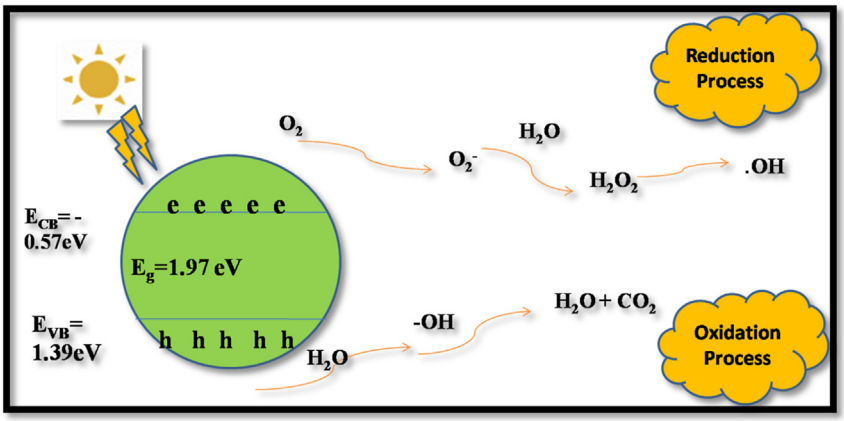

Figure 9. Mechanism of photocatalytic in dye degradation under sunlight irradiation.

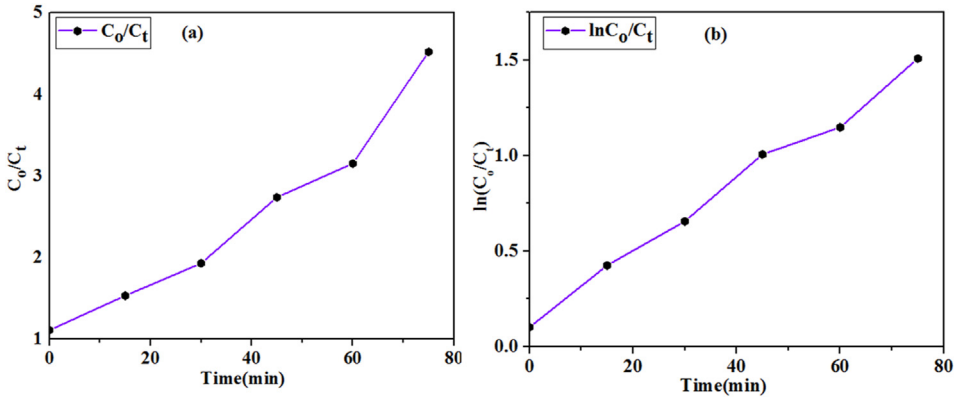

Figure 10. (a) C_o/C_t versus irradiation time (b) Ln (C_o/C_t) versus irradiation time.

between energy eV and (*ahv*). From Tauc plot the value of direct band gap ~1.9 eV.

$$(a\,h\,\upsilon) = B(h\,\upsilon - E\,g)^n \tag{8}$$

In this equation, ν is light frequency, h is Planck constant, α denotes the absorption coefficient, $h\nu$ is energy and E_g is energy of band gap. Band gap is evaluated by intercept of tangent to the X-axis as displayed in Figure 6(b). The value of band gap is estimated about 1.9 eV that suggest that the synthesized sample is suitable for the photodegradation of dye under sunlight irradiation [46, 47].

To estimate the valence and conduction band following Eqs. (9) and (10) are used;

$$E_{CB} = \chi - E^e - 0.5\,Eg \tag{9}$$

$$E_{VB} = E_{CB} + Eg \tag{10}$$

χ is the electronegativity of the synthesized material, E^e is free electrons energy, E_{CB} is conduction band and E_{VB} is valence band potential respectively. The calculated value of conduction band is -0.57 eV, the value of valence band is 1.39 eV and the value of band gap is 1.97 eV.

3.5. Photocatalytic degradation of $AgInSbSe_3$ with Congo red dye

10 ppm solution CR is prepared to check the photocatalytic activity of prepared photocatalyst under direct sunlight. After attaining adsorption-desorption equilibrium condition the sample is placed in sunlight and take sample after every 15 min to check the absorbance of the material.

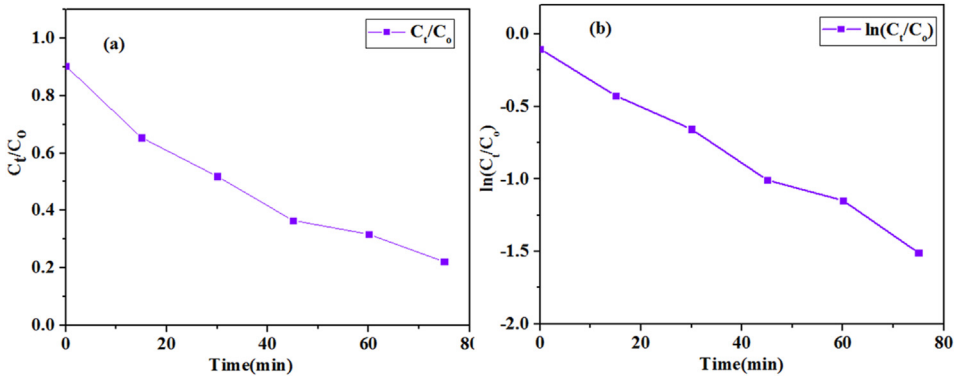

Figure 11. Relative concentration value of dye w. r. t. time (a) C_t/C_o versus time of irradiation time plot (b) $\ln C_t/C_o$ versus time of irradiation plot.

Table 2. Comparison between %age efficiency of selenide based nanomaterials with present work.

Sr. No.	Material	E_g (eV)	Dye	Degradation time	%age Efficiency	References
1	PbSe nanomaterial	2.15	MO	0.5 h	83.13 %	[48]
2	CdSe nanostructured	3.88–1.83	CR	2.5 h	50%	[49]
			MB	4.5 h	88%	
3	$Ba_2AsGaSe_5$	1.39	RhB	2.5 h	23%	[50]
4	bismuth selenide	1.2	RB	2 h	90%	[51]
			CR		35%	
5	Bismuth-cobalt selenide	2.35	CR	1.6 h	85%	[52]
6	$CdSe/CeO_2$	2.61	CR	2.5 h	97.3%	[53]
7	FeSe	2.0	CR	3 h	85.1%	[54]
8	$SrBiSbSe_3$	2.01	CR	1 h	86.9%	[55]
9	$AgInSbSe_3$	1.97	CR	1.25 h	77.8%	Present study

The absorbance reduced constantly as reaction time increased as shown in Figure 7. Figure 7 displays that with the passage of time degradation efficiency increases and reaches to its maximum value after 75 min and its value is 77.8% as shown in Figure 8. To find out the %age degradation efficiency of the material following Eq. (11) is used:

$$\%\text{age degradation (D)} = \frac{C_0 - C_t}{C_0} \times 100 \quad (11)$$

Where, 'D' is the degradation efficiency, C is the Congo red value and C_t stands for the complete time interval absorbance. The result shows that the sample with small value of band gap has appreciable performance under sunlight irradiation is 77.8%.

3.6. Proposed mechanism of photocatalytic degradation of catalyst with Congo red dye

Irradiation of visible light excites the electrons, resulting in the creation of a hole (h^+) in the valence band, which is then transferred to the conduction band (CB) as shown in schematic Figure 9. Both h^+ and electrons migrate to crystal surfaces, where they react with H_2O molecules and molecular oxygen (O_2) to form free superoxide radical anion ($^{\bullet}O^-_2$) and hydroxyl radicals ($^{\bullet}OH$). For photocatalytic degradation of organic pollutants these free radicals acts as active sites as well as potent oxidizing agent.

The following proposed oxidative and reductive reactions may take place in the photocatalytic degradation process of CR dye as shown in Eqs. (12), (13), (14), (15), and (16):

$$AgInSbSe_3 + h\upsilon\ (E > E_g) \rightarrow AgInSbSe_3 + h^+\ (VB) + e^-(CB) \quad (12)$$

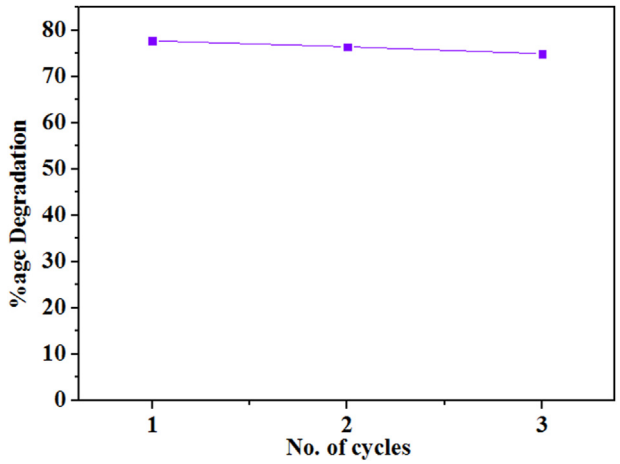

Figure 12. Stability of synthesized photocatalyst after 3 cycles.

$$h^+ + H_2O \rightarrow OH\bullet + H^+ \quad (13)$$

$$h^+ + OH^- \rightarrow OH\bullet \quad (14)$$

$$2H_2O + O_2^- + e^- \rightarrow 2OH + 2OH \quad (15)$$

$$OH\bullet + CR \rightarrow CO_2 + 2H_2O + NO_3^- \quad (16)$$

Finally, these produced hydroxyl radicals degrade the CR dye molecules by converting it into H_2O and CO_2 as byproducts [47].

3.7. Pseudo first order kinetics

The dye solution under direct sunlight more than 1 h without the photocatalyst was revealed no detectable change in the absorbance and color of dye solution. Now we add a measured quantity of catalyst and to achieve adsorption desorption equilibrium kept this dye solution with catalyst under dark for 1 h. The absorbance of CR solution was determined and this is referred as zero time concentration at zero time i.e. Co. After adsorption desorption equilibrium, put sample in direct sunlight and measured dye absorbance was at various time interval and the concentration known as concentration at time t i.e. C_t [21]. Figure 10 (a) and (b) shows the plot (C_o/C_t) and ($\ln C_o/C_t$) intended for the variation during the different concentration against time for the CR degradation under sunlight irradiation over $AgInSbSe_3$. Figure 10 (a) and (b) the reaction profile *vs* time of irradiation. The graph shows an increase with respect to time. In Figure 11 (a) and (b) Kinetic plot of (C_t/C_o) *vs* irradiation time and ln (C_t/C_o) *vs* time t. If we define K_{app} as the pseudo-first order rate constant So the value of rate constant, K_{app}, which is the slope found by the linear fit of the ln (Co/Ct) *vs* irradiation time graph and its value is $K_{app} = 1.80 \times 10^{-2}\ min^{-1}$ of the kinetic plot, gives a qualitative overall assessment of how efficiently a dye is degrading in the presence of a sunlight assisted photocatalyst [47]. In Table 2 comparison between % age efficiency of selenide based nanomaterials with present work has been discussed.

3.8. Stability of the synthesized photocatalyst

To study the stability of the synthesized material under sunlight, 3 successive catalytic experiments has been carried out for 10 ppm CR solution. Centrifugation process has been applied to recycle the catalyst and washed with ethanol and deionized water and dried for 2 h at 180 °C in drying oven. The degradation efficiency of the material decreased from 77.8% to 75% after 3 successive cycles. As shown in Figure 12. A minor deactivation was observed in photocatalytic activity.

4. Conclusion

The silver indium antimony selenide with chemical composition $AgInSbSe_3$ has been prepared via hydrothermal route. The XRD, SEM, EDX, FTIR and UV-vis spectroscopy were made to examine the structure,

morphology, chemical and optical characteristics of the synthesized sample. The average crystalline sizes for $AgInSe_2$ and $AgSbSe_2$ are 19.04 nm and 8.07 nm. SEM image confirms the morphology of the sample that is irregular grains covers the entire homogeneous surface. The calculated grain size of the specimen is 0.58 μm. EDX spectroscopy confirms the presence of antimony, indium, silver and selenium in the sample. FTIR spectroscopy reveals the chemical characteristics of the sample different bands appeared on the graph with wave number ranging from 400-4000 cm^{-1}. From the Tauc plot the band gap was estimated and its value is 1.97 eV. Photocatalytic activity of the $AgInSbSe_3$ has been examined by photocatalytic degradation of CR dye under direct sunlight and showed good degradation 77.8% for CR dye. Kinetics study revealed that $AgInSbSe_3$ follow the pseudo first order kinetics and the value of $K_{app} = 1.80 \times 10^{-2}$ min^{-1}. The synthesized material is also stable and its stability is checked for 3 cycles and minor decrease in %age degradation has been observed. Its stability for photocatalytic activity makes this material a good candidate for degradation of organic pollutants.

Declarations

Author contribution statement

N. Yasmin: Analyzed and interpreted the data; Wrote the paper.

A. Liaqat: Performed the experiments.

G. Ali, A. Kalsoom: Contributed reagents, materials, analysis tools or data.

M. Safdar, M. Mirza: Conceived and designed the experiments; Wrote the paper.

Funding statement

Dr. Misbah Mirza was supported by Higher Education Commission, Pakistan (10408).

Data availability statement

No data was used for the research described in the article.

Declaration of interests statement

The authors declare no conflict of interest.

Additional information

No additional information is available for this paper.

References

[1] N. Ali, S. Ahmad, A. Khan, S. Khan, M. Bilal, S. Uddin, N. Ali, H.M.N. Iqbal, H. Khan, Selenide-chitosan as high-performance nanophotocatalyst for accelerated degradation of pollutants, Chem. Asian J. 15 (2020a).

[2] N. Ali, T.K. Awais, M. Kamal, A. Ul-Islam, S.J. Khan, A. Shah, A. Zada, Chitosan-coated cotton cloth supported copper nanoparticles for toxic dye reduction, Int. J. Biol. Macromol. 111 (2018) 832.

[3] A. Aziz, N. Ali, A. Khan, M. Bilal, S. Malik, N. Ali, H. Khan, Chitosan-zinc sulfide nanoparticles, characterization and their photocatalytic degradation efficiency for azo dyes, Int. J. Biol. Macromol. 153 (2020) 502.

[4] N. Yahya, F. Aziz, N.A. Jamaludin, M.A. Mutalib, A.F. Ismail, W.N.W. Salleh, F. Jaafar, N. Yusof, N.A. Ludin, A review of integrated photocatalyst adsorbents for wastewater treatment, J. Environ. Chem. Eng. 6 (2018) 7411.

[5] M. Anari-Anaraki, A. Nezamzadeh-Ejhieh, Modification of an Iranian clinoptilolite nano-particles by hexadecyltrimethyl ammonium cationic surfactant and dithizone for removal of Pb(II) from aqueous solution, J. Colloid Interface Sci. 440 (2015) 272.

[6] M. Nasrollahzadeh, Z. Issaabadi, S.M. Sajadi, Green synthesis of a Cu/MgO nanocomposite by *Cassytha filiformis* L. extract and investigation of its catalytic activity in the reduction of methylene blue, Congo red and nitro compounds in aqueous media, RSC Adv. 8 (2018) 3723.

[7] Y. Li, S. Guo, H. Yang, Y. Chao, S. Jiang, C.J.R. Wang, One-step synthesis of ultra-long silver nanowires of over 100 μm and their application in flexible transparent conductive films, RSC Adv. 8 (2018) 8057.

[8] Z. Li, G. Wang, K. Zhai, C. He, Q. Li, P. Guo, Methylene blue adsorption from aqueous solution by loofah sponge-based porous carbons, Colloids Surf. A Physicochem. Eng. Asp. 538 (2018) 28.

[9] A. Hernandez-Martínez, et al., Swelling and methylene blue adsorption of poly(N,N-dimethylacrylamide-co-2-hydroxyethyl methacrylate) hydrogel, React. Funct. Polym. 122 (2018) 75.

[10] F. Salimi, S.S. Emami, C. Karami, Removal of methylene blue from water solution by modified nano-boehmite with Bismuth, Inorg. Nano-Metal Chem. 48 (2018) 31.

[11] A. Nezamzadeh-Ejhieh, M. Karimi-Shamsabadi, Decolorization of a binary azo dyes mixture using CuO incorporated nanozeolite-X as a heterogeneous catalyst and solar irradiation, Chem. Eng. J. 228 (2013) 631.

[12] H. Shirzadi, A. Nezamzadeh-Ejhieh, An efficient modified zeolite for simultaneous removal of Pb(II) and Hg(II) from aqueous solution, J. Mol. Liq. 230 (2017) 221.

[13] H. Derikvandi, A. Nezamzadeh-Ejhieh, Designing of experiments for evaluating the interactions of influencing factors on the photocatalytic activity of NiS and SnS_2: focus on coupling, supporting and nanoparticles, J. Colloid Interface Sci. 490 (2017) 628.

[14] Y. Yu, C. Zhao, X. Liu, M. Sui, Y. Meng, Selective focculation of pollutantsin wastewater using pH responsive HM-alginate/chitosan complexes, J. Environ. Chem. Eng. 5 (2017) 5406.

[15] K.H.H. Aziz, et al., Comparative study on 2,4-dichlorophenoxyacetic acid and 2,4-dichlorophenol removal from aqueous solutions via ozonation, photocatalysis and non-thermal plasma using a planar falling film reactor, J. Hazard Mater. 343 (2018) 107.

[16] H. Zhang, G. Xue, H. Chen, X. Li, Magnetic biochar catalyst derived from biological sludge and ferric sludge using hydrothermal carbonization: preparation, characterization and its circulation in Fenton process for dyeing wastewater treatment, Chemosphere 191 (2018) 64.

[17] A.N. Ejhieh, M. Khorsandi, Photodecolorization of Eriochrome Black T using NiS-P zeolite as a heterogeneous catalyst, J. Hazard Mater. 176 (2010) 629.

[18] M. Bahrami, A. Nezamzadeh-Ejhieh, Effect of the supported ZnO on clinoptilolite nano-particles in the photodecolorization of semi-real sample bromothymol blue aqueous solution, Mater. Sci. Semicond. Process. 30 (2015) 275.

[19] A. Raza, et al., Enhanced industrial dye degradation using Co doped in chemically exfoliated MoS 2 nanosheets, Appl. Nanosci. 10 (2020) 1535.

[20] M. Ikram, A. Raza, M. Imran, A. Ul-Hamid, A. Shahbaz, S. Ali, Hydrothermal synthesis of silver decorated reduced graphene oxide (rGO) nanoflakes with effective photocatalytic activity for wastewater treatment, Nanoscale Res. Lett. 15 (1) (2020) 95.

[21] M. Ikram, M.I. Khan, A. Raza, M. Imran, A. Ul-Hamid, S. Ali, Outstanding performance of silver-decorated MoS_2 nanopetals used as nanocatalyst for synthetic dye degradation, Physica 124 (2020), 114246.

[22] M. Aramendia, A. Marinas, J. Marinas, J. Moreno, F. Urbano, Photocatalytic degradation of herbicide fluroxypyr in aqueous suspension of TiO_2, Catal. Today 101 (2005) 187.

[23] Y.Y. Lee, J.H. Moon, Y.S. Choi, G.O. Park, M. Jin, L.Y. Jin, Visible-light driven photocatalytic degradation of organic dyes over ordered mesoporous CdxZn1–xS materials, J. Phys. Chem. C 121 (2017) 5137.

[24] N. Seyedi, K. Saidi, H. Sheibani, Green synthesis of Pd nanoparticles supported on magnetic graphene oxide by Origanum vulgare leaf plant extract: catalytic activity in the reduction of organic dyes and Suzuki–Miyaura cross-coupling reaction, Catal. Lett. 148 (2018) 277.

[25] M. Ikram, et al., 2D chemically exfoliated hexagonal boron nitride (hBN) nanosheets doped with Ni: synthesis, properties and catalytic application for the treatment of industrial wastewater, Appl. Nanosci. 10 (2020) 3525.

[26] S.A. Al Kuhaimi, Z. Tulbah, Structural, compositional, optical and electrical properties of solution-grown zn_x Cd_{1-x} S films, J. Electrochem. Soc. 147 (2000) 214.

[27] P. Intaphong, A. Phuruangrat, K. Karthik, P. Dumrongrojthanath, T. Thongtem, S. Thongtem, Effect of pH on phase, morphology and photocatalytic properties of BiOBr synthesized by hydrothermal method, J. Inorg. Organomet. Polym. Mater. 30 (2019) 714–721.

[28] A. Phuruangrat, P.O. Keereesaensuk, K. Karthik, P. Dumrongrojthanath, N. Ekthammathat, S. Thongtem, T. Thongtem, Synthesis and characterization Ag nanoparticles supported on Bi_2WO_6 nanoplates for enhanced visible-light-driven photocatalytic degradation of rhodamine B, J. Inorg. Organomet. Polym. Mater. 30 (2020) 1033.

[29] A. Phuruangrat, P.O. Keereesaensuk, K. Karthik, P. Dumrongrojthanath, N. Ekthammathat, S. Thongtem, T. Thongtem, Synthesis of Ag/Bi_2MoO_6 nanocomposites using $NaBH_4$ as reducing agent for enhanced visible-light-driven photocatalysis of rhodamine B, J. Inorg. Organomet. Polym. Mater. 30 (2020) 322–329.

[30] A. Sathiya Priyaa, D. Geethaa, K. Karthikb, M. Rajamoorthyc, Investigations on the enhanced photocatalytic activity of (Ag, La) substituted nickel cobaltite spinels, Solid State Sci. 98 (2019), 105992.

[31] K. Kannan, D. Radhika, M.P. Nikolova, V. Andal, K.K. Sadasivuni, S.K. Lakkaboyana, Facile microwave-assisted synthesis of metal oxide CdO-CuO nanocomposite: photocatalytic and antimicrobial enhancing properties, Optik 218 (2020), 165112.

[32] K. Kannan, D. Radhika, S. Vijayalakshmi, K.K. Sadasivuni, A.A. Ojiaku, U. Verma, Facile fabrication of CuO nanoparticles via microwave-assisted method: photocatalytic, antimicrobial and anticancer enhancing performance, Int. J. Environ. Anal. Chem. 102 (2022) 1095–1108.

[33] A.S. Kshirsagar, P.K. Khanna, Titanium dioxide (TiO2) decorated silver indium diselenide (AgInSe2): novel nano-photocatalyst for oxidative dye degradation, Inorg. Chem. Front. 5 (2018) 2242–2256.

[34] D. Ren, O.M. Conanec, V. Dorcetb, M. Cathelinaud, Z. Zheng, H. Ma, X. Zhang, In situ synthesis and improved photoelectric performances of a $Sb_2Se_3/\beta In_2Se_3$,

heterojunction composite with potential photocatalytic activity for methyl orange degradation, Ceram. Int. 46 (2020) 25503–25511.
[35] G. El-Barbary, M.K. Ahmed, M.M. El-Desoky, A.M. Al-Enizi, A.A. Alothman, A.M. Alotaibi, A. Nafady, Cellulose acetate nanofibers embedded with Ag nanoparticles/CdSe/graphene oxide composite for degradation of methylene blue, Synth. Met. 278 (2021), 116824.
[36] M. Dargahzadeh, M. Molaei, M. Karimipour, Completely quenching of the trap states emission of CdSe QDs by CdS/ZnS shell growth using a one pot photochemical approach and application for dye photo-degradation, J. Lumin. 203 (2018) 723–729.
[37] S. Li, M. Zhang, X. Ma, J. Qiao, H. Zhang, J. Wang, Y. Song, Preparation of ortho-symmetric double (OSD) Z-scheme SnO_2\CdSe/Bi_2O_3 sonocatalyst by ultrasonic-assisted isoelectric point method for effective degradation of organic pollutants, J. Ind. Eng. Chem. 72 (2019) 157–169.
[38] Y. Tian, J. Zhang, W. Wang, D. Jia, Ternary 3D framework [Ag5Sn4Se12]3-: solvothermal synthesis, crystal structure and photoelectric properties of an organic silver-rich selenidostannate hybrid, Inorg. Chem. Commun. 131 (2021), 108799.
[39] M. Kulakci, T. Colakoglu, B. Ozdemir, M. Parlak, H.E. Unalan, R. Turan, Silicon nanowires-silver indium selenide heterojunction photodiodes, Nanotechnology 24 (2013), 375203.
[40] K. Hnida, J. Mech, G.D. Sulka, Template-assisted electrodeposition of indium–antimony nanowires – comparison of electrochemical methods, Appl. Surf. Sci. 287 (2013) 252–256.
[41] V.B. Ghanwat, S. Mali, S.S. Bagade, C.S. Mane, R.M. Hong, P.N. Bhosale, Thermoelectric properties of indium(III)-Doped copper antimony selenide thin films deposited using a microwave-assisted technique energy, Technol. 4 (2016) 835–842.
[42] K. Bindu, M.T.S. Nasir, T.K. Das. Roy, P.K. Nasir, Chemically deposited photovoltaic structure using antimony sulfide and silver antimony selenide absorber films, Electrochem. Solid State Lett. 9 (6) (2006) G195.
[43] N. Dulgheru, M. Stoica, J.M. Calderon-Moreno, M. Anastasescu, M. Nicolescu, H. Stroescu, M. Gartner, Optical, morphological and durability studies of quaternary chalcogenide Ge-Sb(As)-(S,Te) films, Mater. Res. Bull. 106 (2018) 234–242.
[44] L. Gharibshahi 1, E. Saion, E. Gharibshahi, A. Shaari, K.A. Matori, Structural and optical properties of Ag nanoparticles synthesized by thermal treatment method, Materials 10 (2017) 402.
[45] S.G. Kumar, K.K. Rao, Comparison of modification strategies towards enhanced charge carrier separation and photocatalytic degradation activity of metal oxide semiconductors (TiO_2, WO_3 and ZnO), Appl. Surf. Sci. 391 (2017) 124–148.
[46] M.N. Ashiq, S. Irshad, M.F. Ehsan, S. Rehman, S. Farooq, M.N. Haq, A. Zia, Visible-light active tin selenide nanostructures: synthesis, characterization and photocatalytic activity, New J. Chem. 41 (2017) 14689–14695.
[47] D.A. Reddy, J. Choi, S. Lee, R. Ma, T.K. Kim, Green synthesis of AgI nanoparticle-functionalized reduced graphene oxide aerogels with enhanced catalytic performance and facile recycling, RSC Adv. 5 (2015) 67394–67404.
[48] M.V. Sharma, H.K. Sharma, N. Jadon, A study on degradation of methyl orange under UV light irradiation and ammonia gas sensing by polypyrrole/lead selenide nanocomposite, Adv. Bio. Res. 12 (2021) 1–12.
[49] N. Ghobadi, P. Sohrabi, H.R. Hatami, Correlation between the photocatalytic activity of CdSe nanostructured thin films with optical band gap and Urbach energy, Chem. Phys. 538 (2020), 110911.
[50] C. Li, X. Li, H. Huang, J. Yao, Y. Wu, Ba2AsGaSe5: a new quaternary selenide with the novel [AsGaSe5] 4–cluster and interesting photocatalytic properties, Inorg. Chem. 54 (2015) 9785–9789.
[51] C. Kulsi, A. Ghosh, A. Mondal, K. Kargupta, S. Ganguly, D. Banerjee, Enhanced photo catalytic performance of nickel doped bismuth selenide under visible light irradiation, Mater. Res. Express 4 (2017), 035902.
[52] S. Khan, A. Khan, N. Ali, S. Ahmad, W. Ahmad, S. Malik, M. Bilal, Degradation of Congo red dye using ternary metal selenide-chitosan microspheres as robust and reusable catalysts, Environ. Technol. Innovat. 22 (2021), 101402.
[53] M.A. Sayed, M.M. Abo-Aly, A.A.A. Aziz, A. Hassan, A.N.M. Salem, A facile hydrothermal synthesis of novel CeO_2/CdSe and CeO_2/CdTe nanocomposites: spectroscopic investigations for economically feasible photocatalytic degradation of Congo red dye, Inorg. Chem. Commun. (2021), 108750.
[54] P. Sohrabi, N. Ghobadi, Optical and photocatalytic behaviors of iron selenide thin films grown by chemical bath deposition versus deposition time and annealing temperature, Appl. Phys. A 125 (2019) 1–11.
[55] Nida, N. Yasmin, A. Kalsoom, H. Qayyum, M. Ahmad, M. Safdar, M. Mirza, Synthesis, Characterization, and photocatalytic activity of quaternary selenide composite using natural sunlight, Optik 251 (2022), 168460.